06

Modification of proton-conducting perfluorinated membranes with graphene oxide

© Yu.V. Kulvelis,[1] V.T. Lebedev,[1] A.V. Shvidchenko,[2] B.B. Tudupova,[1,2] V.I. Kuular,[1,2] N.P. Yevlampieva,[3] E.A. Marinenko,[4] A.S. Odinokov,[5] O.N. Primachenko,[4] I.V. Gofman[4]

[1]St. Petersburg Nuclear Physics Institute, National Research Center Kurchatov Institute,
188300 Gatchina, Russia
[2]Ioffe Institute,
194021 St. Petersburg, Russia
[3]St. Petersburg State University,
199034 St. Petersburg, Russia
[4]Branch of Petersburg Institute of Nuclear Physics named by B.P. Konstantinov of National Research Center „Kurchatov Institute“ — Institute of Macromolecular Compounds,
199004 St. Petersburg, Russia
[5]Russian Scientific Center „Applied Chemistry“,
193232 St. Petersburg, Russia
e-mail: kulvelis_yv@pnpi.nrcki.ru

Received October 12, 2024
Revised October 12, 2024
Accepted October 12, 2024

Composite proton-conducting membranes with graphene oxide based on a perfluorinated copolymer of the Aquivion® type were obtained by casting a mixture of components onto a substrate with subsequent evaporation of the solvent. At fractions of $C_{GO} \geq 0.05$ wt.%, graphene oxide as a modifier in the matrix created large-scale fibril-type structures (cross size ~ 1 mm) with parallel packing on scales ~ 10 mm. Within the fibrils, scanning electron microscopy data revealed a parallel packing of graphene oxide sheets alternating with polymer layers. At $C_{GO} = 0.1$ and 0.2 wt.% tensile tests of samples along the fibrils showed increased elastic modulus and elastic limit relative to the data for transverse deformation. Less modifier fractions (0.02; 0.05 wt.%) caused strengthening, an increase in the deformation resource and proton conductivity (~ 10%, data for 22; 50°C) mainly along the fibrils. The found relationship between the structure, mechanical and conductive properties of composites with variation in the modifier fraction will allow for the targeted design of the membranes, regulating their properties and degree of anisotropy.

Keywords: composites, nanomaterials, layered structures, strength, proton conductivity.

DOI: 10.61011/TP.2025.02.60829.327-24

Introduction

Development of polymer-based membrane materials is important for a wide application range: in hydrogen energy as proton-conductive polyelectrolytes [1–6], chemical techniques of liquid (pervaporation) and gaseous molecular mixture component separation [7–10], medicine (dialysis and oxygen saturation) [11–20].

Possibility of creating new polymer composite materials with various nanoparticles: metal, oxide, carbon structures (fullerenes, nanotubes and nanodiamonds, graphene and its derivatives), is of paramount importance here [21,22]. For introduction into polymer matrices, carbon structures are attractive that they, depending on the task, can be functionalized in multiple ways through grafting atoms and functional groups to them (H, F, OH, COOH, NH_2, SO_3H, etc.) [23–30]. This renders the necessary hydrophilic (hydrophobic) properties to such nanoparticles to form a developed interface with the polymer, where a hybrid diffuse channel network is being created and the desired set of functional properties of membranes is being formed in terms of ion conductivity, selective permeability for atoms and molecules [5–7,21,22,31–35].

Efficiency of nanoparticles as modifiers is defined to a great extent by their specific surface area (S_{SP}). In this case, 2*D*-structures, graphene and its derivatives such as graphene oxide (GO) with record-breaking parameters, $S_{SP}^{G} = 2640\,m^2/g$ [36] and $S_{SP}^{GO} = 2418\,m^2/g$ [37] are the leaders among other commercial carbon forms. Thus, detonation nanodiamonds (DND) have a specific surface area that is almost by an order of magnitude lower $S_{SP}^{DND} \sim 400\,m^2/g$ [38].

In membranes, graphene and GO sheets can create a highly developed interface with a matrix polymer at quite low concentrations due to their high specific surface area. For this, however, it is necessary to provide a particular combination of physical and chemical properties of components such as polarity, availability of functional groups on both sides that are capable of forming hydrogen bonds and/or providing association through charge transfer.

It is particularly important to find methods to form functional hybrid GO-polymer structures as applicable to critical tasks of proton-conductive membrane design — solid polyelectrolytes for hydrogen fuel elements. Currently, despite numerous various polymer ion-exchange membrane designs [39–41], Nafion® perfluorinated copolymer is still the main commercially available material that has long side chains with terminal sulfonic acid groups. Aquivion® material with a similar chemical structure is considered as the nearest alternative [42]. Due to shortened side chains, Aquivion® has improved functional properties compared with its predecessor (Nafion®), though the differences are not fundamental and copolymers have a common origin of ion channel formation for proton transfer [42]. The channels are formed through segregation of sulfonic acid groups that cover the channel interior and form hydrophilic membrane areas. Non-polar backbone copolymer chains form hydrophobic shell around them [43]. By contacting with their shells, cylindrical channels are combined into assemblies (bundles) with locally parallel channel layout, which is supported by the neutron scattering and synchrotron radiation data and reflected in structural ordering models of perfluorinated copolymers [43–53].

Formation of a channel network in perfluorinated copolymers resulting from the interaction of chain fragments (hydrophobic, hydrophilic) and segregation trends, when ion grouping is to any extent combined with partial crystallization of backbone chains, has a probabilistic, rather than regular, nature. Finally, the channel fragments form a coherent, but random, structure that doesn't ensure stability of mechanical and conductive properties of the membrane in the operating conditions at high temperatures and physical loads in harsh chemical environment.

Reinforcement of polymer matrices with 2*D*-carbon structures, for which hydrophilic GO is most suitable, shows promise for improving the functional properties and increasing their resource and stability. Due to hydroxyl groups on the surface, GO can form a 2*D*-conductive interface with sulfonic acid groups of the perfluorinated copolymer, and this interface can serve by itself for proton accumulation and transfer and as an extended platform for binding copolymer ion channels.

The purpose of this work was, firstly, to develop a composite membrane preparation procedure using the Aquivion® type copolymer bound with GO sheets during fabrication of samples from mixed component solutions by casting on polished solid substrates with selection of solvent evaporation modes with a varied amount of modifier. The prepared film composite materials were studied using scanning electron microscopy, uniaxial tension testing, impedance spectroscopy at different temperatures with analysis of possible anisotropic properties in the film plane due to filler structuring in the membranes.

1. Samples and research methods

1.1. Graphene oxide suspension

The stock material consisted of GO aqueous dispersion (0.06 wt.%) prepared by graphite oxidation and exfoliation through the modified Hummers method [54,55]. To achieve the final product, the GO dimethylformamide (DMF) dispersion, aqueous dispersion were subjected to multiple centrifugation, and the collected sediment was dissolved in DMF with water residue removed by centrifugation. In synthesis conditions, ultrasonic treatment of the GO suspension was avoided to prevent GO destruction. Finally, GO DMF dispersions with concentration of 0.81 wt.% and 0.76 wt.% were made, where GO sheets had a negative ξ-potential (-43.3 ± 0.8 mV and -36 ± 3 mV, respectively).

1.2. Copolymer

Perfluorinated copolymer with short side chains Sh-19 (equivalent weight EW = 910 ± 3 g/mol SO_3H) — analogue of commercially available Aquivion® — was synthesized by an aqueous emulsion copolymerization method [56] followed by transfer to sulfonic acid form and preparation of 5% DMF solution to be used in the membrane preparation process [57].

1.3. Membranes

Sh-19 copolymer was used to prepare composite membranes — $\sim 50\,\mu$m thin films with small GO additives (0.02 wt.%, 0.05 wt.%, 0.1 wt.% and 0.2 wt.% with respect to the copolymer — samples Sh19GO002, Sh19GO005, Sh19GO01, Sh19GO02). Mixtures of components dissolved in DMF were casted on the polished glass surface and then the solvent was evaporated at 70°C (casting technique) [58]. A membrane from the pure copolymer without filler (sample Sh19) was prepared in the same way for comparison. A membrane with GO concentration of 0.05 wt.% (sample Sh19GO005T60) was prepared additionally at 60°C to determine the influence of drying temperature on the structure, mechanical and electrokinetic properties of composites.

1.4. Research methods

Membrane samples were examined by the scanning electron microscopy (SEM) method and tested for mechanical and conductive properties. GO surface was tested by SEM using a multifunctional analytical system with crossed ion and electron beams equipped with the GEMINI® electron optical column (Zeiss AURIGA Laser, Carl Zeiss, Jena, Germany) to make SEM images on secondary electron detectors (In-Lens and Everhart-Thornley SE2, (Carl Zeiss, Jena, Germany). The images were processed using SmartSEM® software package (Carl Zeiss, Jena, Germany). Mechanical testing of the membrane films based on the Sh-19 material (identical to Aquivion) were carried out on the AG-100X Plus machine (Shimadzu Corp., Japan) in uniaxial tension

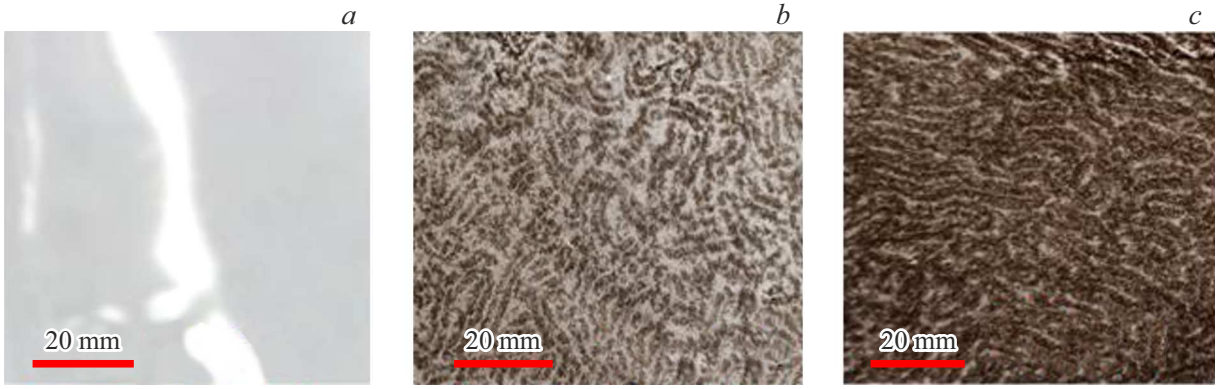

Figure 1. Photographs of membrane surfaces: *a* — Aquivion® type copolymer without filler, *b, c* — copolymer composite materials containing 0.1 wt.% and 0.2 wt.% GO.

mode at a rate of 100 mm/min using samples with a length of 20 mm. Test sample strips were cut from the membranes in two orthogonal directions to evaluate possible anisotropy of mechanical properties. Samples' conductivity was also measured by the impedance spectroscopy method in two orthogonal directions on the film surfaces for anisotropy assessment. Electrokinetic potential analysis of GO particles in DMFA was performed using the Litesizer 500 analyzer (Anton Paar GmbH, Austria).

2. Results and discussion

2.1. Membrane structure

The primary copolymer formed a smooth homogeneous membrane without any visible defects (Figure 1, *a*). In the composite membrane, the filler, starting from 0.05 wt.%, formed a regular system of large-scale inhomogeneities — condensation and rarefaction areas (dark, bright) that are clearly visible in light, which is illustrated by data obtained for typical GO fractions equal to 0.1 wt.% and 0.2 wt.% (Figure 1, *b, c*). The observed dark formations (~ 1 mm in size),saturated GO regions, grouped into fibrils (linear, curved), on the ~ 10 mm scale, laid parallelly at ~ 1 mm intervals. When the GO concentration increased from 0.1 wt.% to 0.2 wt.%, the intervals decreased and the fibril packing density increased together with nematic order strengthening (Figure 1, *b, c*).

Composite structuring indicates that, during the film preparation process as the component mixture was concentrated, the polymer phase got separated from the GO phase when the GO sheets were bonded by the polymer into laminated particles (plates). In solutions, plate overlapping gave rise to fibrils followed by nematic ordering that was fixed during drying of the samples (Figure 1, *b, c*). To understand the nature of the achieved membrane structuring, focus shall be made on kinetic features of membrane preparation process.

Regular morphology of composite materials indicates that, during drying of the samples, solvent diffusion to their surface was more intense between the GO sheets compared with slower solvent molecule migration in the viscous polymer solution. Filler-enriched regions were induced by the fluctuations of GO distribution density in the solution where the GO sheets had the increased effective thickness due to local curving and formed copolymer-depleted 2*D*-channels with fast solvent diffusion. As the solvent was removed, the GO sheets were combined into flaked aggregates, and this process took place faster than the polymer solution got dried, and there was enough time for large GO structures to be formed, that were detected in the membranes (Figure 1, *b, c*). At the same time, it was advantageous for the copolymer chains through sulfonic acid groups to form the polar interface with the GO sheets, which was followed by segregation of polar (non-polar) chain fragments. Hybrid assemblies with alternating GO sheets and non-polar polymer fragment layers were consequently formed. This segregation mechanism differs dramatically from that in the pure copolymer matrix. Ion groups build there linear channels with hydrophobic polymer shells. In a composite material with large surface (GO), plane ion channels shall prevail in lamellas consisting of alternating GO sheets, interface and non-polar polymer layers.

Thus, both composite component ordering mechanisms are associated with the local separation of pure polymer and mixed phases, which altogether facilitates formation of the observed regular composite surface morphology (Figure 1, *b, c*).

Directly on micron (submicron) scales, GO segregation in the polymer matrices was examined using the scanning electron microscopy (SEM) (Figure 2–4). Images of Aquivion® type membrane film (Figure 2) showed 100 nm polymer domains that were previously observed by the SEM and atomic-force microscopy (AFM) methods [57]. Due to GO introduction into the copolymer (0.1 wt.%, 0.2 wt.%), GO clusters occurred in the membranes between free polymer domains (Figure 3, 4). The observed irregular GO particles differed greatly in sizes and geometry due to strong

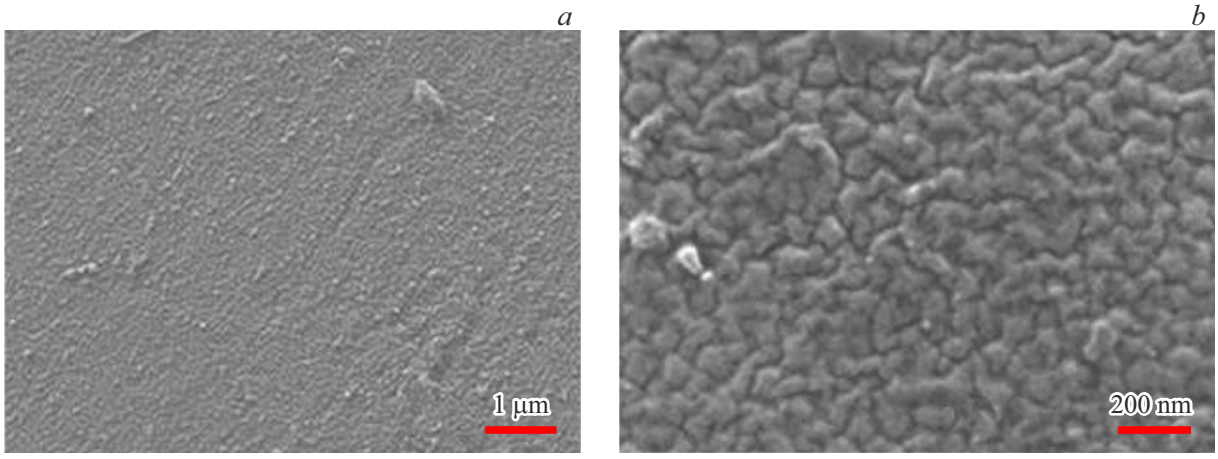

Figure 2. SEM image of the primary copolymer film surface on the 1 μm (a) and 200 nm scales (b).

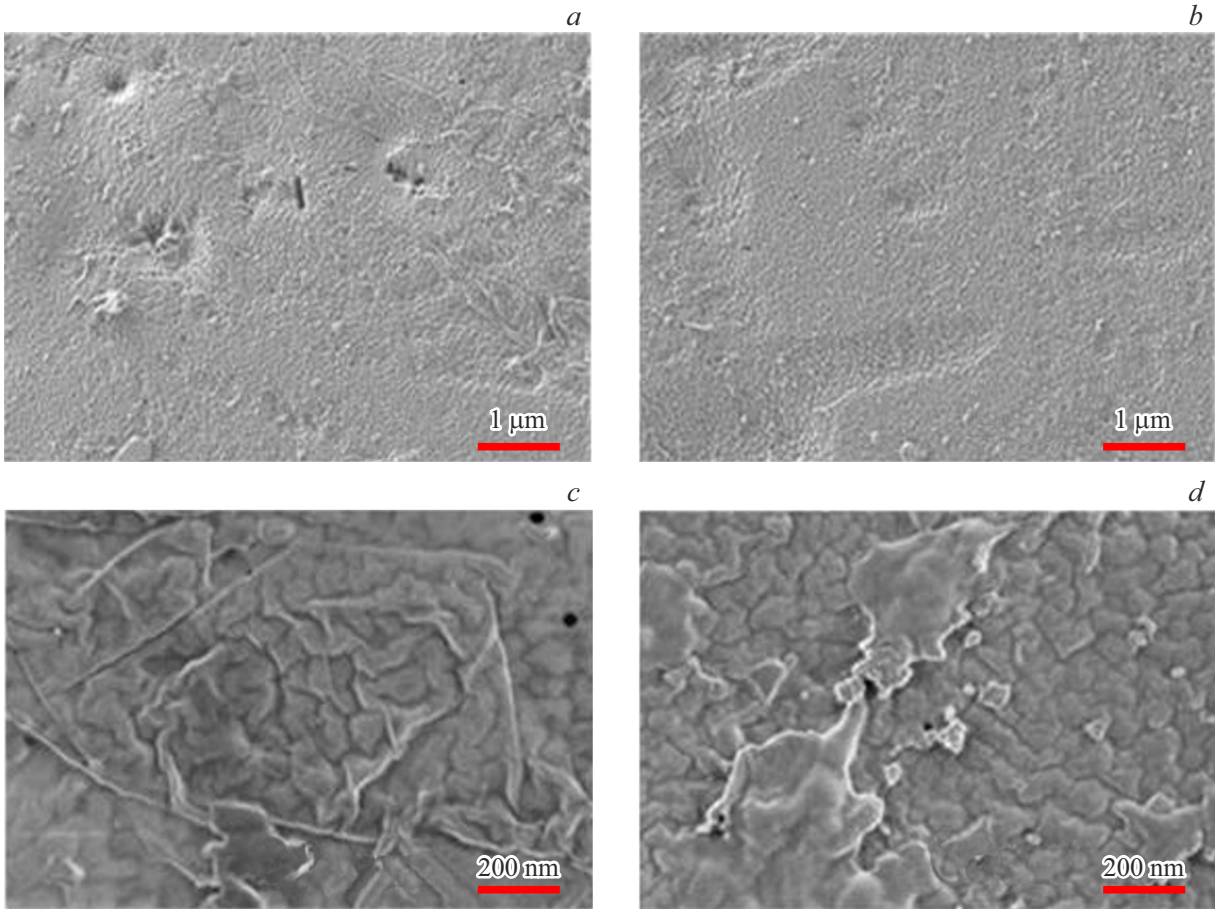

Figure 3. Composite film morphology (0.1 wt.% GO) according to the SEM data: surface areas with modifier (a) and without modifier (b) on the 1 μm scale; c, d — areas with modifier on the 200 nm scale.

copolymer influence on the GO sheet conformation. The GO particles were folded and followed the profile of polar polymer domain boundaries that were covered with them (Figure 3, 4). The above-mentioned composite structuring patterns were also confirmed at low GO concentrations (0.02 wt.%, 0.05 wt.%) (Figure 5).

Composite surface with the minimum GO fraction (0.02 wt.%) in Figure 5, a (scale 1 μm) shows the flaked packing with polymer intervals, and the orientation order in the GO particle layout can be seen (Figure 5, a). GO fragments that cover the polymer domains are observed on a smaller scale (200 nm) (Figure 5, b).

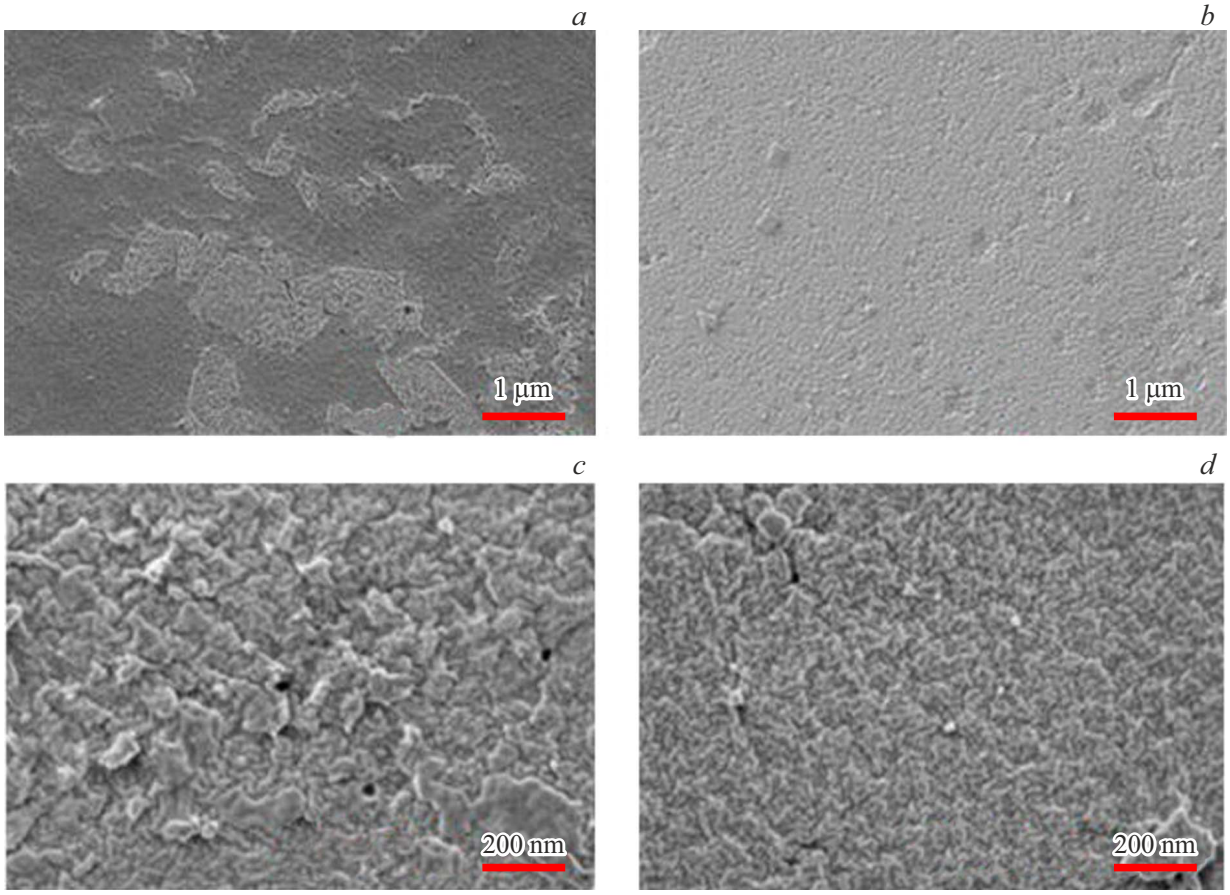

Figure 4. Composite film surface morphology (0.2 wt.% GO, SEM data), areas containing GO (a, c) and without filler (b, d) on the 1 μm (a, b) and 200 nm scales (c, d) are shown.

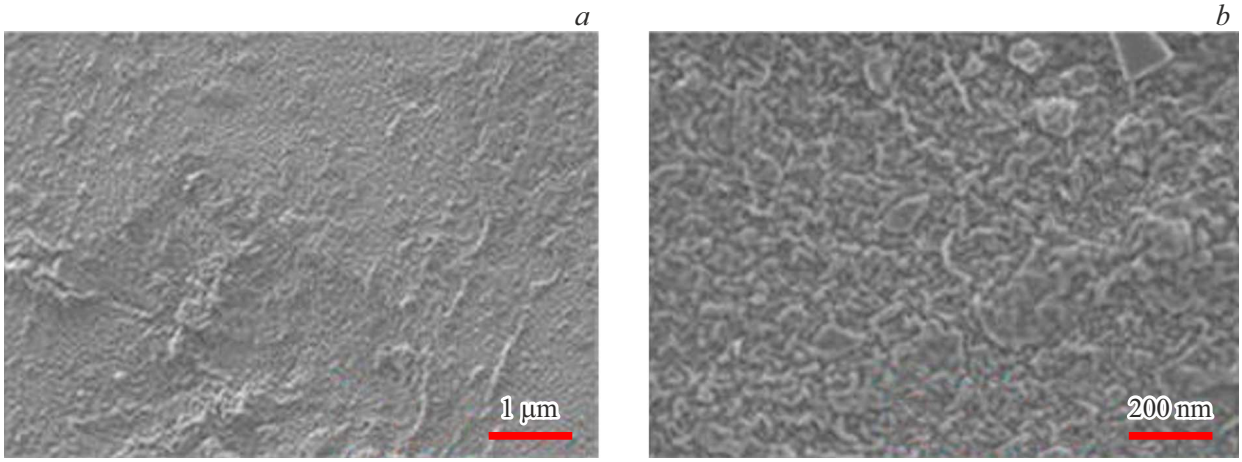

Figure 5. Morphology of a composite film surface with low GO fraction (0.02 wt.%). SEM data on the 1 μm (a) and 200 nm (b) scales.

Enrichment with filler to 0.05 wt.% leads to the membrane surface covered with folded micron-scale GO structures (Figure 6, a) with the presence of areas with small filler inclusions (Figure 6, b). On a smaller scale (200 nm), GO-filled surface domains show convolute GO fragments densely covering the polymer domains (Figure 6, c).

The next experiments found that solvent evaporation temperature plays an important role in membrane morphology formation, which can be seen from data comparison for the sample dried at 70° (Figure 2–6) and 60°C (Figure 7).

The example of a sample containing 0.05 wt.% GO shows that drying temperature reduction facilitates composite

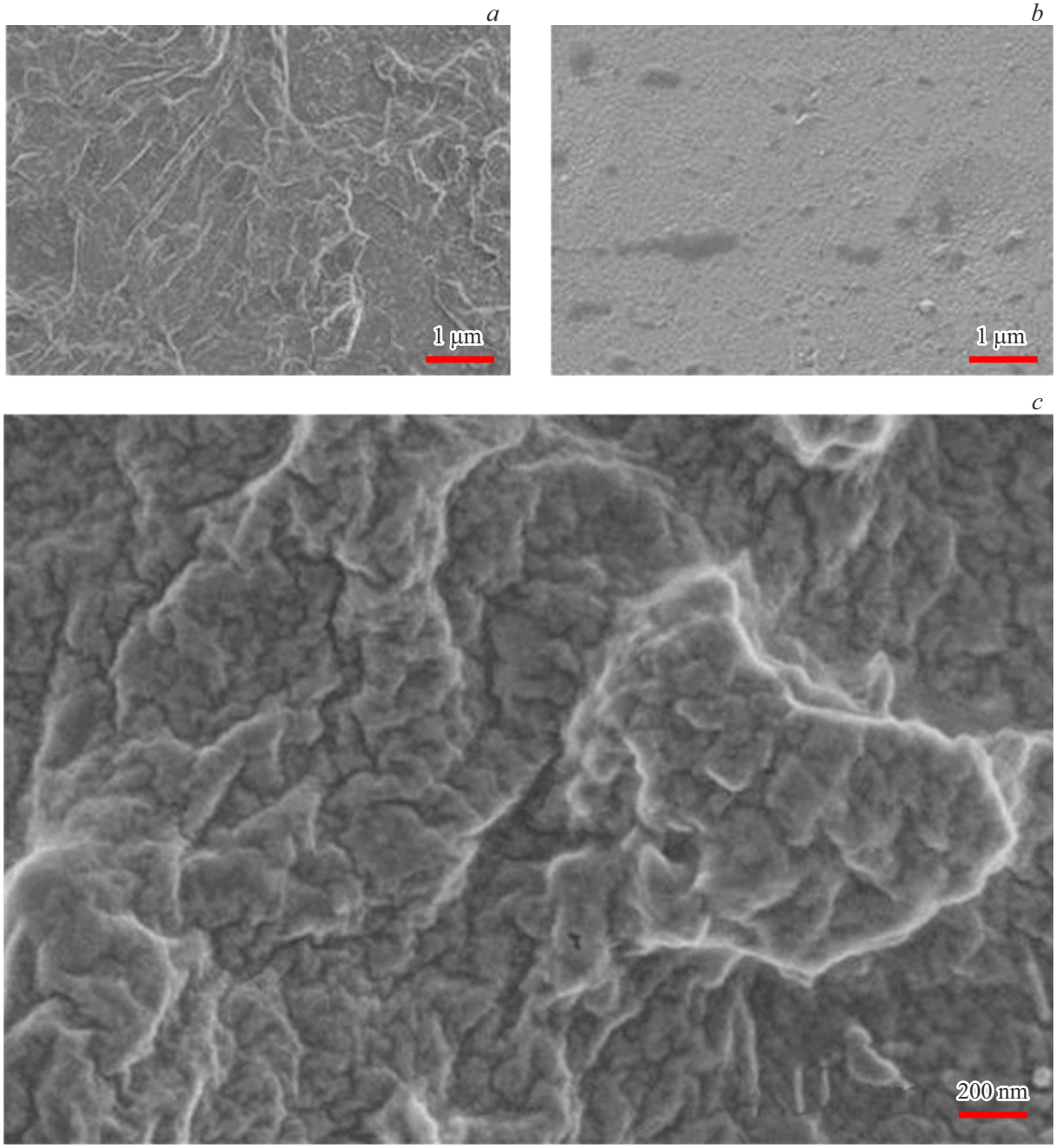

Figure 6. Composite film morphology with GO fraction (0.05 wt.%). SEM images on the 1 μm scale, surface fragments with high content of GO (a) and low content of GO (b), and on the 200 nm scale (c) .

ordering on the submicron scale (Figure 7). In this case, GO sheets cover the polymer domains and acquire folded conformation with a period of $\sim$ 600 nm (Figure 7).

SEM data and macro-level membrane surface morphology observations identified a component ordering mechanism in binary GO and Aquivion® type copolymer composites that is defined as tight binding between the polar fragments of copolymer chains and polar GO surface, thus forming parallel flaked packing of GO sheets with polymer intervals. Ordering effect is more strongly expressed in a membrane prepared from copolymer and GO solution mixture at a lower solvent evaporation temperature (60°C). During sample preparation, component interaction leads to heavy distortion of GO sheet and formation of a developed GO-copolymer interface.

Composite structuring after introduction of small amount of GO into the copolymer matrix affected considerably the stress-strain (strength) properties and ion conductivity of the fabricated materials.

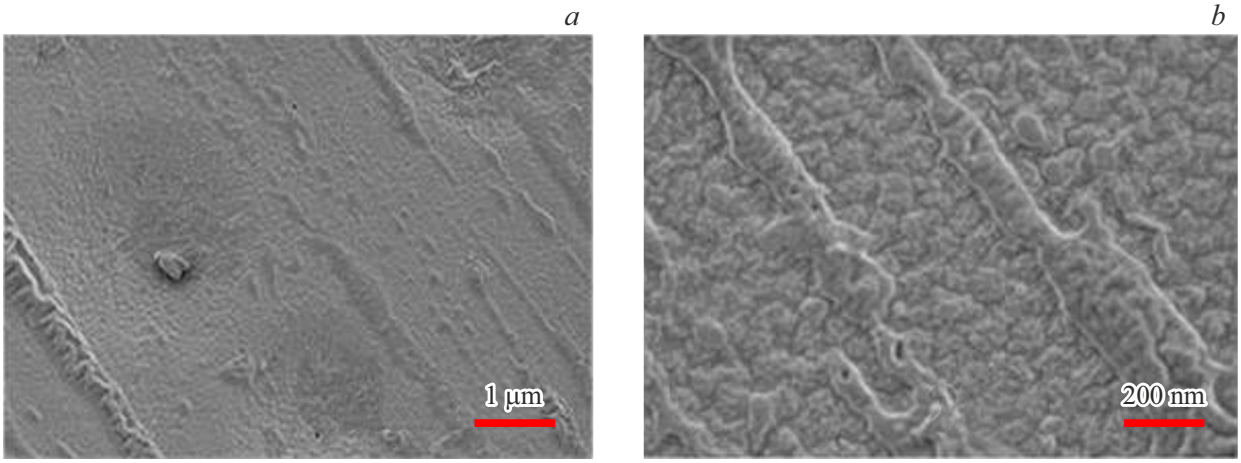

Figure 7. GO ordering in the composite material (0.05 wt.%) dried at 60°C. Data on the 1 μm (a) and 200 nm (b) scales.

2.2. Stress-strain properties of composites

Stress-strain curves of membrane films based on Sh-19 (analogue of Aquivion®) are shown in Figure 8.

Data for the series of composites with GO fractions of 0.02–0.2 wt.% were compared with the data for the sample without filler. To detect a possible anisotropy of stress-strain properties of composite materials due to component segregation, strips were cut from films containing 0.1 wt.% and 0.2 wt.% GO along and across the fibril direction on the film surface (Figure 1), and then performed the tensile test. Using the stress-strain curves (Figure 8), the modulus of elasticity E, plastic limit σ_y, strength σ_b and ultimate deformation to destruction ε_b were determined (Table 1).

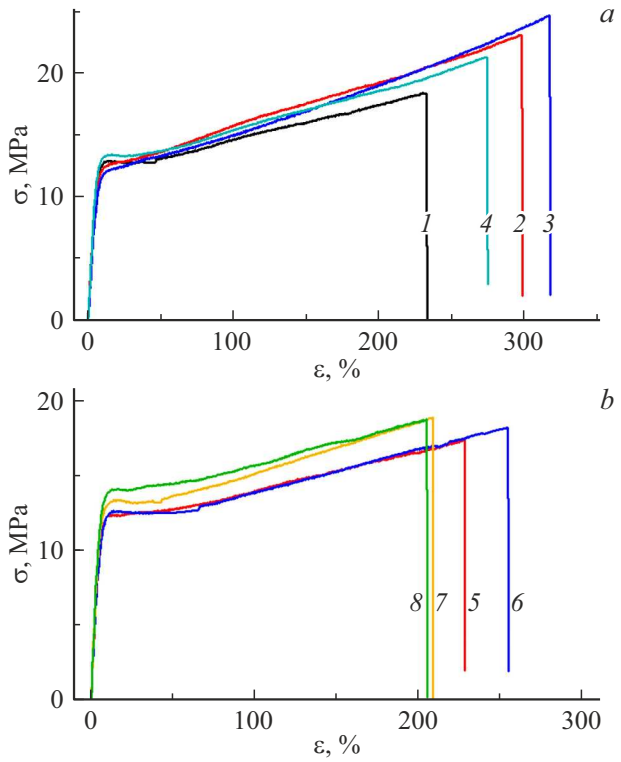

Figure 8. Stress-strain diagrams for membranes: a — film without GO (*1*), composite materials with GO fractions 0.02 wt.% (*2*) and 0.05 wt.%, (*3, 4*); b — composite materials with 0.1 wt.% (*5, 6*) and 0.2 wt.% GO (*7, 8*), measurements in deformation along (*5, 7*) and across (*6, 8*) fibril orientation on the film surface. Data for films made at 70°C (*1, 2, 4–8*) and 60°C (*3*).

Membranes that consisted of low-modulus materials ($E < 270$ MPa) with a relatively narrow deformation resource variation range ($\varepsilon_b = 205 - 317$ %) (Table 1) demonstrated a common strain behavior with crossing the plastic limit at $\varepsilon \sim 6 - 8$ % (sharp reduction of the curve slope) (Figure 8). Curves $\sigma(\varepsilon)$ had no a pronounced domain of waist spreading through the sample and a local maximum corresponding to the plastic limit, and further tension of the samples ($\varepsilon > 10 - 15\%$) took place with a gradual stress growth (strain hardening) (Figure 8).

Then behaviors of the variables found in the initial stress-strain curve segments (modulus of elasticity and plastic limit) were compared for the samples (Figure 9, *a, b*). Concentration dependences $E(C_{GO})$, $\sigma_y(C_{GO})$ demonstrated similarity (Figure 9, *a*) in the series of measurements on the strip samples cut along and across fibrils on the film surface (Figure 9, *a*). This corresponded to a linear correlation between the parameters, $\sigma_y = \alpha + \beta \cdot E$, with the constant α and coefficient $\beta = d\sigma_y/dE$ comparable with the elongation at the transition to plastic deformation (Figure 9, *b*). In case of longitudinal tension, the coefficient $\beta = \beta_P = 0.048 \pm 0.015$ was 30% as high as that for transverse strain $\beta = \beta_t = 0.037 \pm 0.015$. In the first case, fibrils were stretched together with the polymer between them, in the second case, it was enough to elongate the polymer intervals between the fibrils. $\beta_P > \beta_t$ indicates that the fibrils consist of polymer reinforced with GO sheets. Therefore, they are harder than the polymer matrix.

These conclusions were supported by the behavior analysis of other variables — strength and ultimate deformation to destruction (Figure 9, *c, d*).

Table 1. Stress-strain properties of membranes measured at a relative ambient humidity (RH) about 50%

Sample	Composition, thickness, preparation temperature, tension direction	RH, %	E, MPa	σ_y, MPa	σ_b, MPa	$\sigma_b(epsilon)$, %
Sh19	Sh-19, 55–64 μm, 70°C	48	252 ± 11	13.1 ± 0.4	18.4 ± 0.6	236 ± 12
Sh19GO002	Sh-19+0.02 wt.% GO, 65–74 μm, 70°C	49	247 ± 6	12.5 ± 0.4	23.1 ± 1.1	298 ± 18
Sh19GO005T60	Sh-19+0.05 wt.% GO, 54 – 60 μm, 60°C	50	24 ± 12	12.6 ± 0.5	24.7 ± 0.8	317 ± 16
Sh19GO005	Sh-19+0.05 wt.% GO, 66 – 70 μm, 70°C	49	264 ± 9	13.3 ± 0.4	21.5 ± 0.9	276 ± 23
Sh19GO01	Sh-19+0.1 wt.% GO, 63 – 66 μm, 70°C, parallel to fibrils	52	239 ± 12	12.3 ± 0.5	17.5 ± 0.7	227 ± 15
	Sh-19+0.1 wt.% GO, 59 – 63 μm, 70°C, perpendicular to fibrils	54	258 ± 9	12.7 ± 0.4	17.8 ± 0.9	254 ± 12
Sh19GO02	Sh-19+0.2 wt.% GO, 60 ± 63 μm, 70°C, parallel to fibrils	51	257 ± 14	13.5 ± 0.4	19.0 ± 0.9	208 ± 11
	Sh-19+0.2 wt.% GO, 63 ± 66 μm, 70°C, perpendicular to fibrils	53	274 ± 8	13.6 ± 0.1	18.7 ± 0.2	205 ± 12

Note: E — modulus of elasticity, σ_y — plastic limit, σ_b, $\sigma_b(epsilon)$ — strength and ultimate deformation to destruction.

During destruction of the films, the difference between the critical parameters (σ_b, ε_b) (Figure 9, *c*) depending on the sample tension direction is much smaller than that for the modulus of elasticity and plastic limit because destruction is more probable in less strong, mainly polymer, areas of conposite. Thus, in strain along fibrils, the strength (σ_{bp}) is higher on average than in orthogonal tension (σ_{bt}), with a small difference in these quantities $(\sigma_{bp} - \sigma_{bt})/\sigma_{bt} \approx 2\%$. For ultimate strains, the relation is inverse, $\varepsilon_{bt} > \varepsilon_{bp}$, $(\varepsilon_{bt} - \varepsilon_{bp})/\varepsilon_{bp} \approx 3\%$. In both cases, with GO fraction variation (except the upper limit $C_{GO} = 0.2$ wt.%), correlation between the parameters is linear, $\sigma_b = \alpha_b + \beta_b \cdot \varepsilon_b$, with α_b and β_b, values of which for direction along and across the fibrils are almost the same: $\beta_{bp} = 0.079 \pm 0.002$ MPa/%, $\beta_{bt} = 0.078 \pm 0.025$ MPa/% (Figure 9, *d*).

The main result is that quite a small amount of GO (0.05 wt.%) is sufficient to increase the modulus of elasticity and plastic limit, $\Delta E/E_0 \approx 4.8\%$, $\Delta\sigma_y/\sigma_{y0} \approx 1.5\%$, with respect to the pure copolymer and to reinforce the material by increasing the deformation resource, $\Delta\sigma_b/\sigma_{b0} \approx 17\%$, $\Delta\varepsilon_b/\varepsilon_{b0} \approx 17\%$ (Table 1, Figure 9).

Further modification up to 0.1 and 0.2 wt.% leads to high segregation of the carbon component into fibrils (Figure 1) and anisotropy of material stress-strain properties (Figure 9, *a, b*). With such GO fractions, the film's modulus of elasticity (E_t) in tension across fibrils exceeds that (E_p) for longitudinal strain, $(E_t - E_p)/E_p \approx 7.9$ and 6.6%, with plastic limit difference $(\sigma_{yt} - \sigma_{yp})/\sigma_{yp} \approx 3.3$ and 0.7% (Table 1).

Critical parameters also show the anisotropy. In composites (0.1 wt.% GO), strength and ultimate deformation to destruction are equal to $(\sigma_{bt} - \sigma_{bp})/\sigma_{bp} \approx 1.7\%$, $(\varepsilon_{bt} - \varepsilon_{bp})/\varepsilon_{bp} \approx 11.9\%$. However, in samples with dou-

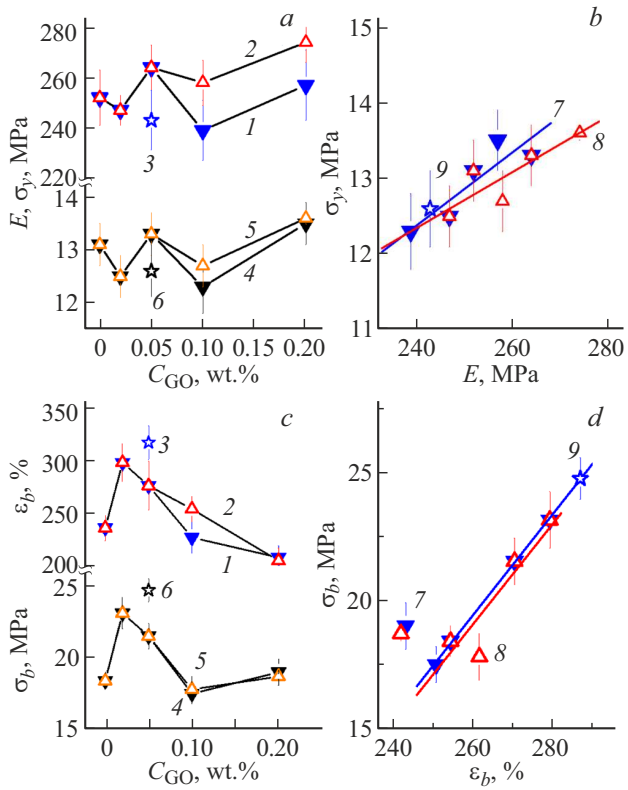

Figure 9. Stress-strain properties of membranes: *a* — modulus of elasticity E (*1–3*) and plastic limit σ_y (*4–6*) depending on the filler fraction C_{GO}; *b* — linear correlation between σ_y and E in the membranes strained along or across the fibrils; *c* — ultimate deformation to destruction ε_b (*1–3*), strength σ_b (*4–6*) of membranes depending on the content of modifier C_{GO}; *d* — correlations of σ_b and ε_b. Curves *1, 4, 7* and *2, 5, 8* — sample deformation data along or across fibrils in membrane series with different content of GO prepared at 70°C; dots *3, 6, 9* — for the composite material (0.05 wt.%) prepared at 60°C.

Table 2. Proton conductivity of membranes (σ) at maximum moisture level depending on the content of GO (C_{GO}), temperature (t), content of absorbed water (W), and measurement directions with respect to fibril orientation

Sample	C_{GO}, wt.%	W, wt.%	σ, S/cm		Direction
			$t = 22°C$	$t = 50°C$	
Sh19	0	34.9	0.125 ± 0.002	0.184 ± 0.004	–
Sh19GO002	0.02	32.3	0.132 ± 0.003	$0.204 - 0.005$	–
Sh19GO005T60	0.05	32.8	0.138 ± 0.004	0.215 ± 0.007	Along
			0.142 ± 0.004	0.219 ± 0.006	Across
Sh19GO005	0.05	33.3	0.133 ± 0.002	0.200 ± 0.004	Along
			0.124 ± 0.003	0.193 ± 0.004	Across
Sh19GO01	0.10	32.5	0.123 ± 0.005	0.197 ± 0.003	Along
			0.123 ± 0.003	0.193 ± 0.005	Across
Sh19GO02	0.20	38.8	0.124 ± 0.005	0.191 ± 0.006	Along
			0.121 ± 0.002	0.204 ± 0.006	Across

bled amount of GO, both parameters showed a negative effect (-1.6, -1.4%, Table 1).

The test results showed that a small GO additive (0.05 wt.%) structured the matrix significantly and improves the set of stress-strain properties of membranes due to binding with copolymer, thus, increasing their modulus of elasticity, plastic limit and strength and extending the strain-to-fracture range, while a higher amount of additive (0.1 wt.%) provides material anisotropy for these variables. Further experiments showed that GO used as a modifier also affects the ion conductivity of membranes just as much.

2.3. Conductivity of composite materials

Proton conductivity of membranes was studied at 22°C and 50°C depending on the content of GO (Figure 10, *a*, Table 2). The membranes were preliminary treated with 15% nitric acid solution (30 min) and rinsed with distilled water to neutral reaction. Then conductivity was measured after boiling of the samples (1 h) with water saturation to a membrane moisture content of 33–39% (Table 2). In films with GO concentrations of $C_{GO} \geq 0.05$ wt.%, fibrils enriched with carbon component were observed, therefore measurements on such samples were performed in directions along and across fibrils for conductivity anisotropy assessment.

As can be seen from concentration dependences $\sigma(C_{GO})$ (Figure 10, *a*), at both temperatures sharp growth of the conductivity (~ 10%) took place when small amounts of GO (0.02–0.05 wt.%) were introduced into the matrix. In the matrix with low GO concentrations, the segregation mechanism of sulfonic acid group chain fragments was kept. They formed ion conductivity channels, and the GO sheets with huge specific surface area bound the channels

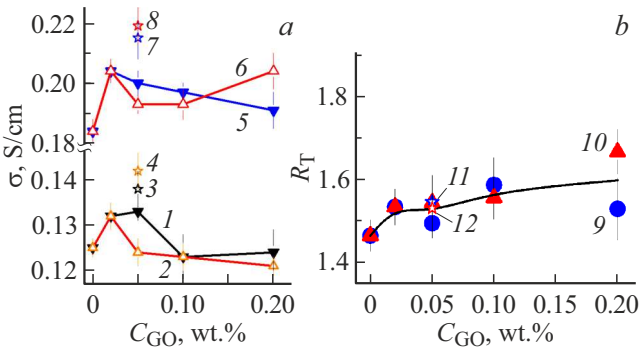

Figure 10. Proton conductivity of membranes: *a* — measured conductivities (σ) with the maximum moisture level depending on the GO concentration (C_{GO}) at 22°C (*1–4*) and 50°C (*5–8*); *b* — conductivity ratio $R_T = \sigma(C_{GO}, 50°C)/\sigma(C_{GO}, 22°C)$ at the specified temperatures depending on the GO concentration in composites, the curve corresponds to the average value over two types of measurements (along and across fibrils). Data *1, 5, 9* was obtained by means of measurements along, *2, 6, 10* — across fibrils for the main sample series (70°C), dots *3, 7, 11* and *4, 8, 12* — similar measurements on the sample prepared at 60°C.

efficiently into a conductive network. Similar patterns were found in perfluorinated copolymer composites with detonation diamonds [32,33,57]. In this case, even a small enrichment with modifier up to 0.1–0.2 wt.% caused the effect reduction due to excessive development of the GO-copolymer interface, which complicated the formation of intrinsic ion channels in the matrix. With moderate content of GO (0.05 wt.%), this was partly compensated by the interface contribution, but only in measurements along the fibrils. In the across direction, the conductivity decreased dramatically and the anisotropy effect was comparable with

the peak conductivity growth with the GO fraction of 0.02 wt.% (Figure 10, *a*). Unlike the membrane series dried at 70°C, the composite material (0.05 wt.%) prepared at 60°C is more conductive due to better matrix ordering with more uniform GO distribution, whereby a higher effect for this sample is observed in the direction across fibrils (Figure 10, *a*).

Copolymer modification causes higher temperature dependence of conductivity according to $R_T = \sigma(C_{GO},\ 50°C)/\sigma(C_{GO},\ 22°C)$. It increases as GO is being added and achieves the growth of $\Delta R_T/R_T(C_{GO} = 0) \sim 10\%$ for measurements along and across the fibril orientation (Figure 10, *b*).

Compared with the primary copolymer in composite materials (0.1−0.2 wt.%), the presence of GO in the matrix increases the proton diffusion activation energy $E_A = \ln(R_T) \cdot k_B/(1/T_1 - 1/T_2)$, where k_B is the Boltzmann constant, T_1 and T_2 are the absolute temperatures in measurements at 22° and 50°C. In composite membranes, the activation energy, $E_{AC} \approx 0.14$ eV, is $\sim 20\%$ as high as $E_{A0} \approx 0.11$ eV in the primary copolymer that is comparable with the properties of similar perfluorinated membranes [1].

Analysis of electrophysical and strength properties of membranes with addition of small amounts of GO showed that all these properties have a common behavior (Figure 9, *c*, 10, *a*). Such similarity is attributable to the fact that GO binding with polymer to form extended fibril-type structures induces anisotropy of conductivity and critical variables (stress and strain to destruction) when the material conductivity and strength along the fibrils become higher than those in the across direction. The former is defined by the developed GO-copolymer interface. It is not only a proton conductor, but also serves for connection of matrix ion channels. On the other hand, flaked component structures reinforce the membrane material, increase its deformation resource, modulus of elasticity and plastic limit (Figure 9) and, thus, reinforce and stabilize the membranes. The obtained results have demonstrated the capabilities of GO as a perfluorinated copolymer modifier that can improve considerably the functional properties of membranes at quite low concentrations due to filler structuring to form hybrid flaked structures with the matrix copolymer.

Conclusion

Approaches have been developed and opportunities have been implemented to prepare Aquivion® type with carbon modifier (GO) by means of deposition of liquid component mixtures onto solid substrates to fabricate and study membrane films containing 0.02−0.2 wt.% GO by the electron microscope, mechanical test and electrophysical measurement methods.

It has been found that, when the solvent evaporated from the films being formed, anisotropic structuring of GO took place by binding with polymer into fibrils packed within the membranes with polymer intervals in the presence of nematic order of fibril orientation. Such fibrillar structures render local anisotropy of stress-strain and conductive properties to membranes where moduli of elasticity and plastic limit are higher along the fibrils and lower in the across direction.

Small modifier fractions (0.02−0.05 wt.%) increase significantly the critical stress and deformation resource of the membrane material. At the same time, membrane conductivity along the fibrils increases due to the developed conductive GO-copolymer interface that also serves as the integrator of intrinsic copolymer ion channels into a coherent stable network for proton migration through the membranes.

The findings are of interest for the development of new membrane materials with modifying carbon structures on the basis of graphene and its derivatives for hydrogen energy sector, selective separation of liquid and gaseous molecular mixtures, effective collection of nuclides from aqueous solutions in nuclear technology.

Acknowledgments

The authors are grateful to L.I. Lisovskaya and I.N. Ivanova or their technical assistance. The authors are grateful to the Resource Center of Nanotechnology of the Saint Petersburg State University for the SEM experiments.

Funding

This study was supported by the Russian Science Foundation (grant No. 23-23-00129).

Conflict of interest

The authors declare no conflict of interest.

References

[1] K.R. Mugtasimova, A.P. Melnikov, E.A. Galitskaya, A.M. Kashin, Yu.A. Dobrovolskiy, G.M. Don, V.S. Likhomanov, A.V. Sivak, V.V. Sinitsyn. Ionics, **24**, 3897 (2018). DOI: 10.1007/s11581-018-2531-5

[2] M. Vinothkannan, A.R. Kim, G.G. Kumar, D.J. Yoo. RSC Adv., **8**, 7494 (2018). DOI: 10.1039/c7ra12768e

[3] B. Barik, A. Kumar, Y. Namgung, L. Mathur, J.-Y. Park, S.-J. Song. Int. J. Hydr. En., **48** (75), 29313 (2023). DOI: 10.1016/j.ijhydene.2023.04.102

[4] J. Ruhkopf, U. Plachetka, M. Moeller, O. Pasdag, I. Radev, V. Peinecke, M. Hepp, C. Wiktor, M.R. Lohe, X. Feng, B. Butz, M.C. Lemme. ACS Appl. Eng. Mater., **1** (3), 947 (2023). DOI: 10.1021/acsaenm.2c00234

[5] R.M.N. Javed, A.Al-Othman, M. Tawalbeh, A.G. Olabi. Renew. Sustain. En. Rev., **168**, 112836 (2022). DOI: 10.1016/j.rser.2022.112836

[6] D. Ion-Ebrasu, B.G. Pollet, A. Spinu-Zaulet, A. Soare, E. Carcadea, M. Varlam, S. Caprarescu. Int. J. Hydr. En., **44** (21), 10190 (2019). DOI: 10.1016/j.ijhydene.2019.02.148

[7] M.V. Gudkov, D.Yu. Stolyarova, K.A. Shiyanova, V.P. Mel'nikov. Polymer Science, Series C, **64**, 40 (2022). DOI: 10.1134/S1811238222010027
[8] D.A. Gkika, V. Karmali, D.A. Lambropoulou, A.C. Mitropoulos, G.Z. Kyzas. Membranes, **13**, 127 (2023). DOI: 10.3390/membranes13020127
[9] A. Kausar, I. Ahmad, T. Zhao, O. Aldaghri, M.H. Eisa. Processes, **11**, 927 (2023). DOI: 10.3390/pr11030927
[10] E.O. Ezugbe, S. Rathilal. Membranes, **10**, 89 (2020). DOI: 10.3390/membranes10050089
[11] C. Lavorato, E. Fontananova. Microorganisms, **11**, 310 (2023). DOI: 10.3390/microorganisms11020310
[12] Y. Kan, J.V. Bondareva, E.S. Statnik, E.V. Koudan, E.V. Ippolitov, M.S. Podporin, P.A. Kovaleva, R.R. Kapaev, A.M. Gordeeva, J. Cvjetinovic, D.A. Gorin, S.A. Evlashin, A.I. Salimon, F.S. Senatov, A.M. Korsunsky. Int. J. Mol. Sci., **24**, 6255 (2023). DOI: 10.3390/ijms24076255
[13] A. Ali, M.I. Vohra, A. Nadeem, B.S. Al-Anzi, M. Iqbal, A.A. Memon, A.H. Jatoi, J. Akhtar, J. Yang, K.H. Thebo. ACS Appl. Polym. Mater., **6** (8), 4747 (2024). DOI: 10.1021/acsapm.4c00285
[14] F. Dorey, L.A. Furer, S. Zehnder, R. Furrer, R. Brönnimann, I. Shorubalko, T. Buerki-Thurnherr. J. Mater. Chem. B, **11** (42), 10097 (2023). DOI: 10.1039/D3TB01784B
[15] A.K. Evseev, S.V. Zhuravel, A.Yu. Alentiev, I.V. Goroncharovskaya, S.S. Petrikov. Membr. Membr. Technol., **1** (4), 201 (2019). DOI: 10.1134/S2517751619040024
[16] P.L. Ivanov, A.Yu. Alentyev, S.V. Chirkov. *Membrane hollow fiber blood oxygenator* (Patent RU 2 750 524 C1, 2020) (in Russian)
[17] E. Pasqualotto, E. Cretaio, M. Scaramuzza, A. De Toni, L. Franchin, A. Paccagnella, S. Bonaldo. Biosensors, **12** (12), 1079 (2022). DOI: 10.3390/bios12121079
[18] V.V. Zhmakin, S.Yu. Markova, V.V. Teplyakov, M.G. Shalygin. Membr. Membr. Technol., **5** (2), 107 (2023). DOI: 10.1134/s2517751623020087
[19] M. Schalenbach, T. Hoefner, P. Paciok, M. Carmo, W. Lueke, D. Stolten. J. Phys. Chem. C, **119** (45), 25145 (2015). DOI: 10.1021/acs.jpcc.5b04155
[20] Y. Cheng, C.I. Moraru. Colloids Surf. B: Biointerfaces, **162**, 16 (2018). DOI: 10.1016/j.colsurfb.2017.11.016
[21] R. Wilson, G. George, A.J. Jose. In: *New polymer nanocomposites for environmental remediation*, eds. C.M. Hussain, A.K. Mishra (Elsevier Inc., 2018), Ch. 18, p. 457. DOI: 10.1016/B978-0-12-811033-1.00018-4
[22] S.F. Nitodas, M. Das, R. Shah. Membranes, **12**, 454 (2022). DOI: 10.3390/membranes12050454
[23] E.N. Karaulova, E.I. Bagrii. Rus. Chem. Rev., **68** (11), 889 (1999). DOI: 10.1070/RC1999v068n11ABEH000499
[24] T.P. Dyachkova, A.G. Tkachev *Methods of functionalization and modification of carbon nanotubes* (Spektr, M., 2013) (in Russian). 152 s. ISBN 978-5-4442-0050-6
[25] A.E. Aleksenskii. In: *Detonation Nanodiamonds. Science and Applications*, eds. A.Y. Vul, O.A. Shenderova (Pan Stanford Publishing, Danvers, MA, USA, 2014), p. 37–72.
[26] A. Aleksenskii, M. Bleuel, A. Bosak, A. Chumakova, A. Dideikin, M. Dubois, E. Korobkina, E. Lychagin, A. Muzychka, G. Nekhaev, V. Nesvizhevsky, A. Nezvanov, R. Schweins, A. Shvidchenko, A. Strelkov, K. Turlybekuly, A. Vul', K. Zhernenkov. Nanomaterials, **11** (8), 1945 (2021). DOI: 10.3390/nano11081945
[27] O.V. Tomchuk, V. Ryukhtin, O. Ivankov, A.Ya. Vul', A.E. Aleksenskii, L.A. Bulavin, V.L. Aksenov, M.V. Avdeev. Fuller. Nanotub. Carbon Nanostructures, **28** (4), 272 (2020). DOI: 10.1080/1536383X.2019.1697686
[28] A.V. Petrov, K.N. Semenov, I.V. Murin. Russ. J. Gen. Chem., **90** (5), 927 (2020). DOI: 10.1134/S1070363220050308
[29] I.I. Kulakova, G.V. Lisichkin. Russ. J. Gen. Chem., **90** (10), 1921 (2020). DOI: 10.1134/S1070363220100151
[30] D. Chen, H. Feng, J. Li. Chem. Rev., **112** (11), 6027 (2012). DOI: 10.1021/cr300115g
[31] V.N. Postnov, N.A. Melnikova, G.A. Shulmeister, A.G. Novikov, I.V. Murin, A.N. Zhukov. Russ. J. Gen. Chem., **87** (11), 2754 (2017). DOI: 10.1134/S1070363217110391
[32] V.T. Lebedev, Y.V. Kulvelis, A.V. Shvidchenko, O.N. Primachenko, A.S. Odinokov, E.A. Marinenko, A.I. Kuklin, O.I. Ivankov. Membranes, **13**, 850 (2023). DOI: 10.3390/membranes13110850
[33] V.T. Lebedev, Yu.V. Kulvelis, A.S. Odinokov, O.N. Primachenko, S.V. Kononova, E.M. Ivan'kova, V.A. Orlova, N.P. Yevlampieva, E.A. Marinenko, I.V. Gofman, A.V. Shvidchenko, G.S. Peters. J. Membr. Sci. Lett., **4** (1), 100070 (2024). DOI: 10.1016/j.memlet.2024.100070
[34] D.M. Sterescu, L. Bolhuis-Versteeg, N.F.A. van der Vegt, D. Stamatialis, M. Wessling. Macromol. Rapid Comm., **25** (19), 1674 (2004). DOI: 10.1002/marc.200400296
[35] A.F. Yazid, H. Mukhtar, R. Nasir, D.F. Mohshim. Membranes, **12** (6), 589 (2022). DOI: 10.3390/membranes12060589
[36] P. Kamedulski, M. Skorupska, P. Binkowski, W. Arendarska, A. Ilnicka, J.P. Lukaszewicz. Sci. Rep., **11**, 22054 (2021). DOI: 10.1038/s41598-021-01154-0
[37] S.K. Kandasamy. In: *Graphene, Nanotubes and Quantum Dots-Based Nanotechnology. Fundamentals and Applications* (Woodhead Publishing Series in Electronic and Optical Materials, 2022), Ch. 8, p. 155–172. DOI: 10.1016/B978-0-323-85457-3.00024-4
[38] A.Ya. Vul, A.T. Dideikin, A.E. Aleksenskiy, M.V. Baidakova. In: *Nanodiamond, RSC Nanoscience and Nanotechnology*, ed. O.A. Williams (RSC Publishing, Cardiff, 2014)
[39] A.B. Yaroslavtsev, I.A. Stenina. Mendeleev Commun., **31** (4), 423 (2021). DOI: 10.1016/j.mencom.2021.07.001
[40] A.B. Yaroslavtsev, I.A. Stenina, D.V. Golubenko. Pure Appl. Chem., **92** (7), 1147 (2020). DOI: 10.1515/pac-2019-1208
[41] Z. Cui, E. Drioli, Y.M. Lee. Prog. Polym. Sci., **39** (1), 164 (2014). DOI: 10.1016/j.progpolymsci.2013.07.008
[42] T. Li, J. Shen, G. Chen, S. Guo, G. Xie. ACS Omega, **5** (28), 17628 (2020). DOI: 10.1021/acsomega.0c02110
[43] K. Schmidt-Rohr, Q. Chen. Nat. Mater., **7**, 75 (2008). DOI: 10.1038/nmat2074
[44] A. Eisenberg. Macromolecules, **3** (2), 147 (1970). DOI: 10.1021/ma60014a006
[45] A. Eisenberg, B. Hird, R.B. Moore. Macromolecules, **23** (18), 4098 (1990). DOI: 10.1021/ma00220a012
[46] M. Fujimura, T. Hashimoto, H. Kawai. Macromolecules, **15** (1), 136 (1982). DOI: 10.1021/ma00229a028
[47] G. Gebel. Macromolecules, **33** (13), 4850 (2000). DOI: 10.1021/ma9912709
[48] A.-L. Rollet, O. Diat, G. Gebel. J. Phys. Chem. B., **106** (12), 3033 (2002). DOI: 10.1021/jp020245t
[49] L. Rubatat, G. Gebel, O. Diat. Macromolecules, **37** (20), 7772 (2004). DOI: 10.1021/ma049683j
[50] G. Gebel, O. Diat. Fuel Cells, **5** (2), 261 (2005). DOI: 10.1002/fuce.200400080
[51] K.-D. Kreuer. Chem. Mater., **26** (1), 361 (2014). DOI: 10.1021/cm402742u
[52] K.-D. Kreuer, G. Portale. Adv. Funct. Mater., **23** (43), 5390 (2013). DOI: 10.1002/adfm.201300376

[53] J.A. Elliott, D. Wu, S.J. Paddison, R.B. Moore. Soft Matter, **7**, 6820 (2011). DOI: 10.1039/C1SM00002K
[54] W.S. Hummers, R.E. Offeman. J. Am. Chem. Soc., **80**, 1339 (1958). DOI: 10.1021/ja01539a017
[55] M.K. Rabchinskii, A.D. Trofimuk, A.V. Shvidchenko, M.V. Baidakova, S.I. Pavlov, D.A. Kirilenko, Yu.V. Kulvelis, M.V. Gudkov, K.A. Shiyanova, V.S. Koval, G.S. Peters, V.T. Lebedev, V.P. Melnikov, A.T. Dideikin, P.N. Brunkov. Tech. Phys., **67** (12), 1611 (2022). DOI: 10.21883/TP.2022.12.55197.208-22
[56] O.N. Primachenko, A.S. Odinokov, E.A. Marinenko, Y.V. Kulvelis, V.G. Barabanov, S.V. Kononova. J. Fluor. Chem., **244**, 109736 (2021). DOI: 10.1016/j.jfluchem.2021.109736
[57] O.N. Primachenko, Yu.V. Kulvelis, A.S. Odinokov, N.V. Glebova, A.O. Krasnova, L.A. Antokolskiy, A.A. Nechitailov, A.V. Shvidchenko, I.V. Gofman, E.A. Marinenko, N.P. Yevlampieva, V.T. Lebedev, A.I. Kuklin. Membranes, **12** (9), 827 (2022). DOI: 10.3390/membranes12090827
[58] O.N. Primachenko, A.S. Odinokov, V.G. Barabanov, V.P. Tyul'mankov, E.A. Marinenko, I.V. Gofman, S.S. Ivanchev. Russ. J. Appl. Chem., **91**, 101 (2018). DOI: 10.1134/S1070427218010160

Translated by E.Ilinskaya